

## Stress history influence on sedimentary rock porosity estimates: Implications for geological CO<sub>2</sub> storage in Northern Taiwan

Wen-Jie Wu<sup>1</sup>, Jia-Jyun Dong<sup>1,2,\*</sup>, Andrew Tien-Shun Lin<sup>2</sup>, Yun-Chen Yu<sup>3</sup>, Tsun-You Pan<sup>2</sup>, Lun-Tao Tong<sup>4</sup>, Ming-Hsu Li<sup>5</sup>, Chuen-Fa Ni<sup>1</sup>, and Toshihiko Shimamoto<sup>6</sup>

<sup>1</sup> Graduate Institute of Applied Geology, National Central University, Taoyuan City, Taiwan

<sup>2</sup> Department of Earth Sciences, National Central University, Taoyuan City, Taiwan

<sup>3</sup> Institute of Nuclear Energy Research, Atomic Energy Council, Taoyuan City, Taiwan

<sup>4</sup> Green Energy and Environment Research Laboratories, Industrial Technology Research Institute, Hsinchu, Taiwan

<sup>5</sup> Graduate Institute of Hydrological and Oceanic Sciences, National Central University, Taoyuan City, Taiwan

<sup>6</sup> State Key Laboratory of Earthquake Dynamics, Institute of Geology, China Earthquake Administration, Beijing, China

### Article history:

Received 10 August 2012

Revised 25 September 2012

Accepted 21 September 2015

### Keywords:

CO<sub>2</sub> storage capacity, Deep saline aquifer, Porosity-depth relation, Effective stress, Stress history, Injection pressure

### Citation:

Wu, W.-J., J.-J. Dong, A. T.-S. Lin, Y.-C. Yu, T.-Y. Pan, L.-T. Tong, M.-H. Li, C.-F. Ni, and T. Shimamoto, 2017: Stress history influence on sedimentary rock porosity estimates: Implications for geological CO<sub>2</sub> storage in Northern Taiwan. *Terr. Atmos. Ocean. Sci.*, 28, 247-258, doi: 10.3319/TAO.2015.09.21.03(GSC)

### ABSTRACT

We established a stress-history-dependent porosity model of potential target rocks for CO<sub>2</sub> geosequestration based on rock sample porosity measurements under various effective stresses (5 - 120 MPa). The measured samples were collected from shallow boreholes (< 300 m depth) drilled at the frontal fold in northern Taiwan. The lithology, density, and the stress-history-dependent porosity derived from shallow boreholes enabled us to predict the porosity-depth relationship of given rock formations at (burial depths of approximately 3170 - 3470 m) potential sites for CO<sub>2</sub> geosequestration located near the Taoyuan Tableland coastline. Our results indicate that the porosity of samples derived from laboratory tests under atmospheric pressure is significantly greater than the porosity measured under stress caused by sediment burial. It is therefore strongly recommended that CO<sub>2</sub> storage capacity assessment not be estimated from the porosity measured under atmospheric pressure. Neglecting the stress history effect on the porosity of compacted and uplifted rocks may induce a percentage error of 7.7% at a depth of approximately 1000 m, where the thickness of the eroded, formerly overlying formation is 2.5 km in a synthetic case. The CO<sub>2</sub> injection pressure effect on the porosity was also evaluated using the stress-history-dependent porosity model. As expected, the pore pressure buildup during CO<sub>2</sub> injection will induce an increase in the rock porosity. For example, a large injection pressure of 13 MPa at a depth of approximately 1000 m will increase the rock porosity by a percentage error of 6.7%. Our results have implications for CO<sub>2</sub> storage capacity injection pressure estimates.

## 1. INTRODUCTION

Carbon dioxide capture and storage (CCS) is a promising technology for reducing anthropogenic CO<sub>2</sub> emissions into the atmosphere (Bachu 2000; Lackner 2003; Wilson et al. 2003; IPCC 2005; Bachu et al. 2007; Bradshaw et al. 2007). CO<sub>2</sub> storage in geological media is considered the most efficient technology that can be readily applied to significant CO<sub>2</sub> subsurface sequestration (Bachu 2008). Many pilot test sites (e.g., Frio Brine Pilot Experiment, US,

Kharaka et al. 2006) and commercial CO<sub>2</sub> storage sites (e.g., Sleipner, offshore Norway, Torp and Gale 2004) have been successfully developed, confirming the maturity of CO<sub>2</sub> geosequestration technology.

Predicting the CO<sub>2</sub> storage capacity and the migration of the injected CO<sub>2</sub> plume is central to CO<sub>2</sub> geosequestration. The rock permeability and porosity are two critical parameters that govern the CO<sub>2</sub> storage capacity and plume migration (Juanes et al. 2006; Bachu et al. 2007). Conventional laboratory experiments (e.g., the imbibition method) and core logging are typically used to evaluate the rock porosity under atmospheric pressure. However, rocks at depth

\* Corresponding author  
E-mail: jjdong@geo.ncu.edu.tw

are subjected to stresses. Borehole logging is frequently used to evaluate the rock porosity at depth and to establish a porosity-depth relationship in a given borehole (e.g., Lin et al. 2003). The influence of the stress history (such as sediment burial, uplift by folding and faulting, and subsequent exhumation) on the porosity of a given rock succession (Wu and Dong 2012) is difficult to evaluate using these methods. The CO<sub>2</sub> reservoir pore volume may vary through time during and after CO<sub>2</sub> injection due to changes in pore pressures. A method to evaluate the stress-history-dependent porosity, taking into account the pressure buildup effect from CO<sub>2</sub> injection, is therefore required.

There are few studies on CO<sub>2</sub> plume migration (e.g., Oldenburg et al. 2001; Xu et al. 2006; Birkholzer and Zhou 2009; Lengler et al. 2010) and the hydro-mechanical issues involved in CO<sub>2</sub> leakage risk assessments and reservoir stability (e.g., Rutqvist and Tsang 2002; Rutqvist et al. 2007, 2008, 2010; Rohmer and Seyedi 2010; Vilarrasa et al. 2010; Morris et al. 2011). However, study on the dependence of storage capacity upon the stress has attracted little attention. We present the stress-dependent porosities of sedimentary rocks based on laboratory measurements. The samples were collected from boreholes drilled at the frontal fold of the Western Foothills in northern Taiwan. The frontal fold is approximately 20 km east of potential CO<sub>2</sub> geosequestration sites near the Taoyuan Tableland coastline. Equivalent potential CO<sub>2</sub> cap and reservoir rocks near the Taoyuan coastline are exposed along the frontal fold due to thrusting and subsequent erosion. We developed a method using logging data from a shallow well and a stress-history-dependent porosity model to predict the porosity-depth relationship in a deeper reservoir at potential CO<sub>2</sub> geosequestration sites. The influence of the in-situ stress, maximum overburden and injection pressure on the porosity is carefully depicted and discussed. Our results have implications for CO<sub>2</sub> storage capacity injection pressure estimates.

## 2. STRESS-HISTORY-DEPENDENT POROSITY

It has long been recognized that the porosity of sedimentary rocks decreases with increasing depth (e.g., Athy 1930). Based on laboratory experimental results, Dong et al. (2010) proposed a power-law function to describe the relationship between rock porosity ( $\phi$ ) and effective stress ( $\sigma_e$ ):

$$\phi = \phi_o (\sigma_e / \sigma_o)^{-q} \quad (1)$$

where  $\phi_o$  is the initial porosity of sediment under atmospheric pressure ( $\sigma_o$ ) and  $q$  is a material constant. Wu and Dong (2012) suggested that the maximum overburden stress (i.e., stress history) strongly controls the porosity of sedimentary rocks experiencing uplift and subsequent erosion. The poros-

ity of an overconsolidated rock unloaded from its maximum effective stress ( $\sigma_{pc}$ ) may be expressed as follows:

$$\phi = \phi_{pc} (\sigma_e / \sigma_{pc})^{-q'} \quad (2)$$

where  $\phi_{pc}$  [equal to  $\phi_o \cdot (\sigma_{pc} / \sigma_o)^q$ ] is the porosity under  $\sigma_{pc}$  and  $q'$  is a material constant. The general form of the stress-history-dependent porosity of the sedimentary rocks may be expressed as

$$\phi = \phi_o \cdot (\sigma_{pc} / \sigma_o)^{-q} \cdot (\sigma_e / \sigma_{pc})^{-q'} \quad (3)$$

When  $\sigma_{pc} = \sigma_e$  (i.e., the effective stress at present equals the maximum past effective stress), Eq. (3) will be identical to Eq. (1). In other words, if the sedimentary rocks are normally consolidated, then their porosity may be evaluated using Eq. (1).

The stress history dependence of sedimentary rocks is illustrated in Fig. 1. Circles in Fig. 1a denote the measured porosities of rocks loaded and unloaded. Wu and Dong (2012) found that the data points may be divided into three groups, namely a recompaction group (RC, blue circles), virgin-compaction group (VC, purple circles), and decompaction group (DC, red circles). Each group displays a linear trend in a log-log plot, and the data points from each group may be fitted along a straight line. The intersection of the RC group and VC group lines indicates the maximum past overburden stress sustained by the rocks, which is related to the maximum burial depth of the rocks. The porosities of the VC group may be described using Eq. (1), with the calibrated constants  $\phi_o$  and  $q$  (intercept and slope of the fitted line of the VC group). The porosities of the RC and DC groups are a function of the maximum past overburden ( $\sigma_{pc}$ ) the rocks experienced, which can be evaluated using Eq. (3) if the  $\sigma_{pc}$  and  $q'$  (slopes of the fitted lines of RC or DC groups) can be further determined.

When CO<sub>2</sub> is injected into the target formation, the pore pressure increases and the effective stress decreases. This process will result in an unloading effect, leading to an increase in the porosity, which can be described using the stress-history-dependent porosity model proposed by Wu and Dong (2012). The normally consolidated rocks (i.e., no uplift and erosion since sediment deposition) may therefore become overconsolidated. Figure 1b illustrates variations in the porosity of normally consolidated rocks with various effective confining stresses (i.e., various depths) on a log-log plot during the CO<sub>2</sub> injection. If the rocks have never experienced uplift and erosion prior to CO<sub>2</sub> injection the porosities of the rocks at various depths will then plot along a line describing normal sediment compaction. The initial porosity of sediment under atmospheric pressure is  $\phi_o$ . When we retrieve a rock specimen at a depth  $d$  with porosity  $\phi_v$ ,

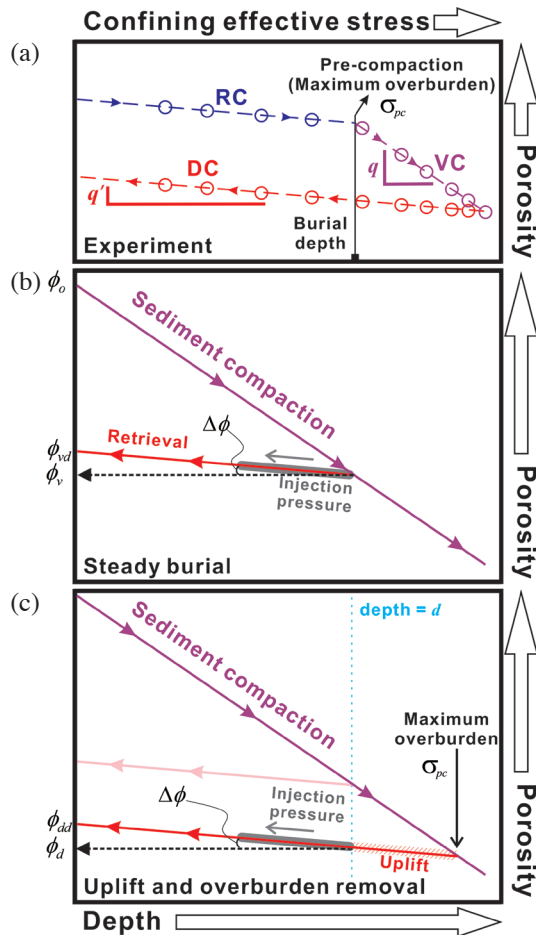


Fig. 1. (a) Illustration of typical porosity curves shown on a log-log plot of porosity measurements from compacted rocks. There are three types of porosity curves: recompaction curve (dashed blue line, RC), virgin-compaction curve (dashed purple line, VC), and decompaction curve (dashed red line, DC). (b) Compaction curve for normally consolidated rocks due to increasing overburden. If the rock is brought to the surface, it is unloaded and the porosity increases. The porosity increases in response to an increase in pore pressure because of CO<sub>2</sub> injection. (c) Porosity curve for an over-consolidated rock. Variation in porosities due to CO<sub>2</sub> injection ( $\Delta\phi$ ) increases with increasing injection pressure.

the rock will be unloaded to atmospheric pressure when we bring it to the surface and its porosity increases to  $\phi_{vd}$ . Note that the porosity measured using a downhole logging tool at in-situ stress will be  $\phi_v$ . During CO<sub>2</sub> injection, the effective rock stress decreases by the amount of the injection pressure according to the effective stress principle (Terzaghi 1943). Accordingly, the porosity increases as the rocks are unloaded. The injection-induced porosity variation ( $\Delta\phi$ ) is a function of the injection pressures (increases with increasing injection pressure).

Figure 1c illustrates the porosity variations with CO<sub>2</sub> injection in rock formations that experienced uplift after their maximum burial (i.e., uplifted to depth  $d$ ). The porosity of the rock ( $\phi_d$ ) will be less than that of normally con-

solidated rock ( $\phi_v$ ) at an identical depth  $d$ . If the rock is retrieved from a depth  $d$  and brought to the surface, the rock is unloaded and its porosity under atmospheric pressure will be equal to  $\phi_{vd}$ . The rock porosity at depth measured using downhole logging tools will be  $\phi_d$ . As in the case of normally consolidated rocks, the porosity of an overconsolidated rock will increase by  $\Delta\phi$  with the injection of CO<sub>2</sub> into the target formations.

The target formations for CO<sub>2</sub> injection in saline aquifers should be deeper than approximately 800 m (Benson and Cole 2008). Deep reservoir rocks at sites favorable for CO<sub>2</sub> geosequestration are often unavailable for laboratory testing during the site screening stage. We had the advantage that equivalent reservoir rocks had been uplifted by thrusting along the nearby frontal fold-and-thrust belt. The porosity-depth relationship in reservoir rocks at the CO<sub>2</sub> geosequestration sites could be evaluated using a stress-history-dependent porosity model developed in the laboratory. Meanwhile, the potential influence of pore pressure accumulation due to injection could also be assessed.

### 3. REGIONAL GEOLOGIC SETTING AND METHODOLOGY

#### 3.1 Regional Geologic Setting

The study area is located in a belt of frontal folding in northern Taiwan (Fig. 2a), near potential CO<sub>2</sub> geosequestration sites in the Taihsi Basin (TB) near the Taoyuan coastline. The late Miocene to early Pliocene Kueichulin Formation (KCL) and the late Miocene Nanchuang Formation (NC) are potential CO<sub>2</sub> reservoirs. Figure 2a shows a depth-contour map of the NC Formation top (or base of the KCL Formation) proposed by Lin and Watts (2002), and Fig. 2b shows the structures and stratigraphy in an E-W-oriented cross section.

To investigate the characteristics of the potential CO<sub>2</sub> reservoirs and seal rocks, a 300-m deep borehole, designated Sanying-1 (SY-1, red star in Fig. 2a), and several shallow boreholes a few meters deep were drilled in the hanging wall of the Hsinchuang Fault to retrieve potential reservoir rock samples from the NC and KCL Formations potential seal rocks of the Chinshui Shale. A sedimentological log of the SY-1 cores was developed. These cores were scanned using a multi-sensor core logger to measure their radioactivity (i.e., gamma-ray log) and bulk density (Fig. 3).

Figure 2b shows that the potential CO<sub>2</sub> reservoirs near the coast lie slightly deeper than approximately 1000 m. However, equivalent potential reservoirs are exposed or shallowly buried in the frontal fold due to folding and reverse faulting along the Hsinchuang Fault. The influence of uplift and erosion on the porosity was evaluated in this study based on the laboratory-derived porosity model, which took into consideration the stress history dependence.

### 3.2 Samples and Laboratory Experiments

Eleven samples, including six sandstone and five mudstone, were used to measure the sample porosities under various confining stresses. Eight samples (SY1-01 ~ SY1-08) from the KCL and NC Formations were taken from Sanying-1 borehole cores (Fig. 3). Three rock samples (SB3-01, SB3-02, and SB4-01) were taken from cores from two shallow boreholes, SB-3 and SB-4 (both were 10 m deep), near the Sanying-1 borehole where the Chinshui Shale is exposed. Descriptions of all of the tested samples are listed in Table 1. All of the tested rock samples were homogeneous and intact.

We used an integrated permeability/porosity measurement system (YOKO2) to measure the rock sample porosities (Wang et al. 2009; Dong et al. 2010; Wu and Dong 2012). The tests were performed using an intra-vessel oil-pressure apparatus at room temperature. A pressure generator with an oil apparatus was used to raise the confining stress to 200 MPa. The sample was jacketed into two heat shrinkable polyolefin tubes 1-mm in thickness to prevent

the confining oil from flowing into the sample. The sample porosity was obtained from the balanced pore gas pressure after two airtight spaces with the initial pressures were connected. Detailed descriptions of the equipment and sample preparation process can be found in Dong et al. (2010).

### 3.3 Estimation of Porosity-Depth Relationship of Potential CO<sub>2</sub> Reservoirs

For potential CO<sub>2</sub> geosequestration preliminary evaluation the deep target formation parameters are always not available. Data from shallow boreholes or outcrops related to the target formation near the potential CO<sub>2</sub> reservoir are sometimes used for such evaluations. A new method was developed in this study for predicting the porosity-depth relationship in deeper potential CO<sub>2</sub> reservoirs using logging data from shallower boreholes and a stress-history-dependent porosity model. We illustrate the evaluated porosity-depth relationship for the lower part of the KCL Formation and the upper part of the NC Formation at locations near the coastline and in the Taoyuan Tableland.

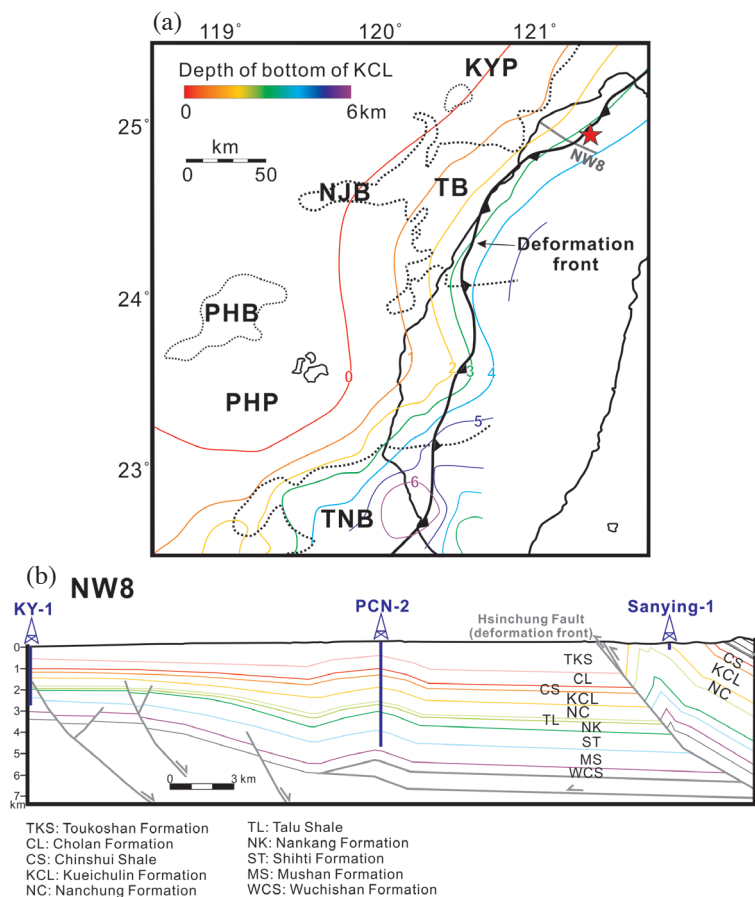


Fig. 2. (a) Depth-contour map showing depths to the contact between the Kueichulin (KCL) and Nanchuang (NC) Formations (modified from Lin and Watts 2002). The red star denotes the location of well Sanying-1. The thick gray line denotes the NW8 profile location shown in (b). TB: Taihsi Basin; KYP: Kuanyin Platform; NJB: Nanjihtao Basin; PHB: Penghu Basin; PHP: Penghu Platform; TNB: Tainan Basin. (b) Geological profile (NW8) across the frontal fold and the Taoyuan Tableland (Yang et al. 2003). Location of well Sanying-1 is projected onto this section.

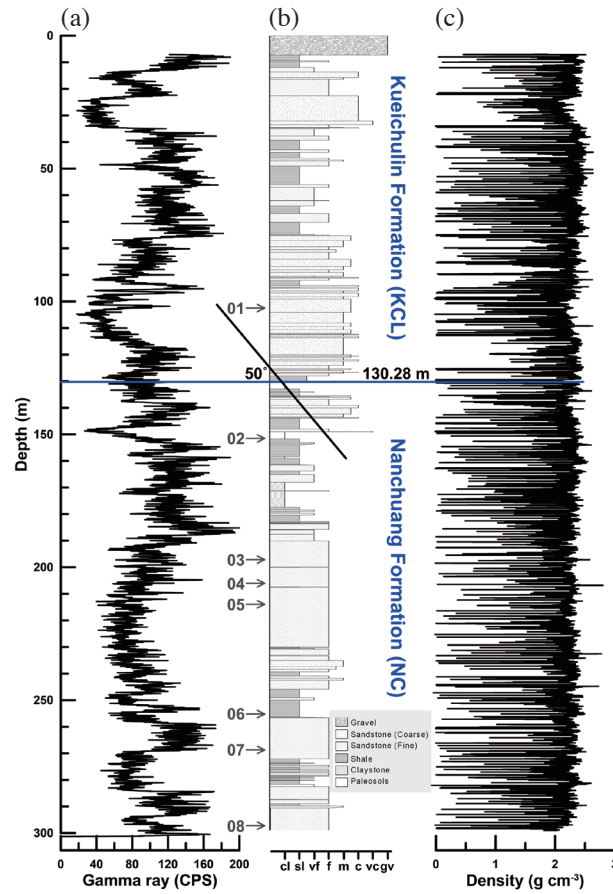


Fig. 3. A stratigraphic column (-7 ~ -300 m) and measurements performed using a multi-sensor core logger in well Sanying-1. (a) Gamma-ray log, (b) sedimentological log, and (c) density log. Bedding dip in the cores is approximately 50°, and the contact between the KCL and NC Formations is at a depth of 130.28 m. The density and gamma-ray measurements were recorded at 2- and 10-cm sampling intervals, respectively. Stratigraphic positions of the tested rock samples are indicated by arrows shown in (b). (Color online only)

Table 1. Physical parameters, lithologies, rock formations, and ages of all tested samples.

| No.    | Borehole | Depth (m) | Diameter/Length (mm) | Dry density <sup>#</sup> (g cm <sup>-3</sup> ) | Lithology           | Formation      | Epoch    |
|--------|----------|-----------|----------------------|--|---------------------|----------------|----------|
| SB3-01 | SB-3     | 3.55      | 8.19/25.21           | 2.23   | Shale               | Chinshui Shale | Pliocene |
| SB3-02 | SB-3     | 6.45      | 11.84/25.46          | 2.28   | Shale               |                |          |
| SB4-01 | SB-4     | 8.31      | 11.67/25.37          | 2.23   | Shale               |                |          |
| SY1-01 | SY-1     | 100.85    | 20.10/25.16          | 1.78   | Sandstone (C*)      | Kueichulin Fm. | Miocene  |
| SY1-02 | SY-1     | 149.90    | 17.82/25.14          | 2.00   | Mudstone (paleosol) | Nanchuang Fm.  |          |
| SY1-03 | SY-1     | 195.50    | 15.65/25.50          | 1.88   | Sandstone (F*)      |                |          |
| SY1-04 | SY-1     | 204.41    | 12.12/25.46          | 1.88   | Sandstone (F*)      |                |          |
| SY1-05 | SY-1     | 212.32    | 24.88/25.02          | 1.86   | Sandstone (F*)      |                |          |
| SY1-06 | SY-1     | 253.61    | 14.23/25.50          | 2.32   | Shale               |                |          |
| SY1-07 | SY-1     | 267.10    | 16.61/25.36          | 2.03   | Sandstone (F*)      |                |          |
| SY1-08 | SY-1     | 295.58    | 12.11/25.35          | 2.07   | Sandstone (F*)      |                |          |

Note: \*: C: Coarse grained; F: Fine grained. #: Dry density is derived from laboratory experiment.

There may be suitable sites for CO<sub>2</sub> geosequestration near well KY-1, as shown in Fig. 2b. The contact between the KCL and NC Formations is at a depth of 1323 m in well KY-1 (Chiu 2009). This contact is at a depth of 130.28 m below the ground surface and 123.28 m beneath the terrace gravels base (which are 7 m thick) in borehole Sanying-1 (Fig. 3). Using the NC-KCL contact in boreholes KY-1 and Sanying-1 as a datum plane, the top of the KCL Formation was projected to a depth of 1199.72 m (1323 - 123.28 m) in borehole Sanying-1. This interval was considered a potential CO<sub>2</sub> geosequestration site. The base of the drilled NC Formation in borehole Sanying-1 was projected to be at a depth of 1492.72 m (1199.72 + 293 m).

Based on the measured porosity of the rocks in shallow borehole Sanying-1 (total depth 300 m), the stress-history-dependent porosity model [Eq. (3)] can be derived. The rock parameters ( $\phi_o$ ,  $q$ , and  $q'$ ) from various lithologies required in Eq. (3) can be obtained from the test results from over-consolidated rocks in the hanging wall of the Hsinchung Fault. The lithology and in-situ overburden stress are essential parameters for evaluating the porosity-depth relationship of potential CO<sub>2</sub> reservoirs in normally consolidated rocks. The gamma-ray log of borehole Sanying-1 and the lithology observed by visually examining the cores, which can be projected to the depth of the potential CO<sub>2</sub> reservoirs (i.e., well KY-1), are illustrated in Figs. 3a and b. The density log can be used to estimate the in-situ overburden of the potential CO<sub>2</sub> reservoirs. The in-situ effective vertical stress  $\sigma_e$  at depth can be calculated using the equation

$$\sigma_e = \int_0^z \rho'(\tau) \cdot d\tau \quad (4)$$

where  $\rho'$  is the submerged density, which equals the density of the saturated sediment minus the water density. The rock densities at depths between 1199.72 and 1492.72 m in the potential CO<sub>2</sub> reservoirs are available from the multi-sensor core logger measurements in borehole Sanying-1 (Fig. 3c). The rock densities above 1199.72 m are from Wu and Dong (2012), and the thicknesses of the formations in well KY-1 are from Chiu (2009). Table 2 summarizes the average rock densities and formation thicknesses of the KCL Formation and the overlying formations.

## 4. RESULTS

### 4.1 Porosity Curves vs. Effective Confining Stress and Stress-History-Dependent Porosity Model

The measured porosities of eleven rock samples are presented on a log-log plot (Fig. 4). All of the samples were loaded to 120 MPa and reloaded, with the exception of sample SY1-01 as this coarse-grained sandstone was poorly cemented. Sample SY1-01 was loaded to 80 MPa and then subsequently reloaded. The porosities of six sandstones range

between 11.86 and 28.89% under the test confining stresses. As expected, the porosities of the poorly cemented coarse-grained sandstones are significantly higher than those of the other tested and more compacted sandstones. The porosities for four shales range between 7 and 10.99% under confining stresses ranging from 5 - 120 MPa. The porosities of the fine-grained paleosols range from 10.61 - 17.74% and are significantly greater than those of the shale samples.

As indicated in Fig. 1, the porosity curve versus effective confining stress obtained with increasing load stresses can be modeled as two linear functions [Eqs. (1) and (3)] on a log-log plot; their intersection yields the maximum overburden pressure (i.e., the maximum past burial depth that the rock experienced). Accordingly, the stress history (maximum overburden) effect on the porosity was determined. Based on the measured porosities of the samples and

Table 2. The bulk density and thickness of formations above the NC Formation, from Chiu (2009) and Wu and Dong (2012).

| Formation                          | TKS* | CL*   | CS*   | KCL*  |
|------------------------------------|------|-------|-------|-------|
| Thickness (m)                      | 331  | 552   | 128   | 312   |
| bulk density (g cm <sup>-3</sup> ) | 2.1  | 2.425 | 2.538 | 2.446 |

Note: \*: TKS: Toukoshan Formation; CL: Cholan Formation; CS: Chinshui Shale; KCL: Kueichulin Formation.

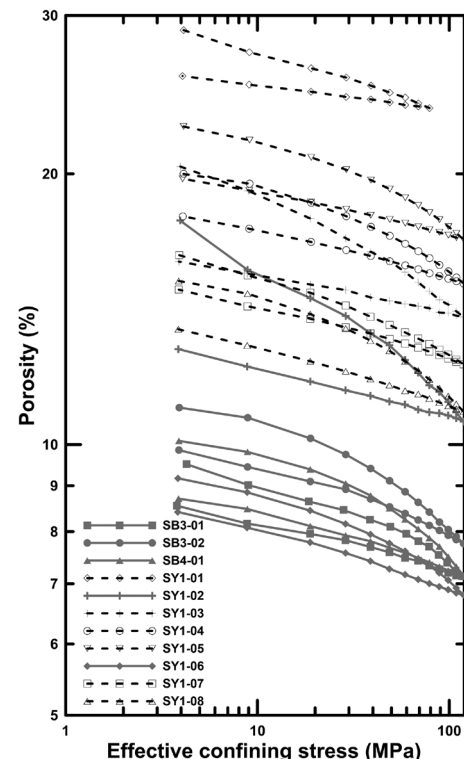


Fig. 4. Compaction curves for eleven tested sedimentary rocks. Dashed lines denote sandstones and solid lines denote shales and paleosol.

the linear regressions developed using Eqs. (1) and (3), the maximum effective stress ( $\sigma_{pc}$ ), the initial porosity of the sediment ( $\phi_o$ ) under atmospheric pressure and material constants  $q$  and  $q'$  can be determined, as shown in Table 3. Notably, the maximum overburden ( $\sigma_{pc}$ ) of the rocks along the KCL-NC contact is 44.03 MPa, estimated based on a burial depth of 3300 m shown on the contour map of Lin and Watts (2002) and an average bulk density of 2.36 g cm<sup>-3</sup> (Wu and Dong 2012). The average stress,  $\sigma_{pc}$ , of eight tested samples is approximately 47.09 MPa, which is close to the value determined using the geological data discussed above.

#### 4.2 Porosity-Depth Relationship of Deep CO<sub>2</sub> Reservoirs Predicted Using Shallow Borehole Data

As mentioned earlier, data from shallow boreholes or outcrops related to the target formation near the potential CO<sub>2</sub> reservoir are sometimes used in preliminary evaluations of potential CO<sub>2</sub> geosequestration. In this section, we describe using the data derived from a shallow borehole to determine the porosity-depth relationship of a deep target formation. Lateral variations in sedimentary facies are neglected in this demonstration of the proposed technique. In the present case, the stresses imposed by strata overlying the target formations in the shallow borehole were substantially reduced due to tectonic uplift and erosion. Accordingly, the

stress-history-dependent porosity model derived from the rock cores from the shallow borehole (over-consolidated rocks) was used to estimate the porosity-depth relationship of the target formation (normally consolidated rocks).

The in-situ vertical stresses in rocks lying between 1199.72 and 1492.72 m below the ground surface were calculated using Eq. (4); with the results shown in Fig. 5a. The

Table 3. Parameters obtained from rock experiments performed in this study.

| No.    | Lithology      | $\sigma_{pc}$ (MPa) | $\phi_o$ (%) | $q$   | $q'$  |
|--------|----------------|---------------------|--------------|-------|-------|
| SB3-01 | Shale          | 63.52               | 25.56        | 0.181 | 0.056 |
| SB3-02 | Shale          | 39.08               | 26.03        | 0.166 | 0.070 |
| SB4-01 | Shale          | 36.72               | 25.68        | 0.176 | 0.057 |
| SY1-01 | Sandstone (C*) | 52.44               | 43.74        | 0.092 | 0.028 |
| SY1-02 | Paleosol       | 51.87               | 53.95        | 0.230 | 0.055 |
| SY1-03 | Sandstone (F*) | 42.41               | 43.51        | 0.162 | 0.043 |
| SY1-04 | Sandstone (F*) | 43.77               | 45.23        | 0.134 | 0.043 |
| SY1-05 | Sandstone (F*) | 49.35               | 40.13        | 0.133 | 0.048 |
| SY1-06 | Shale          | 59.12               | 21.77        | 0.160 | 0.060 |
| SY1-07 | Sandstone (F*) | 28.82               | 25.50        | 0.160 | 0.053 |
| SY1-08 | Sandstone (F*) | 48.96               | 37.58        | 0.170 | 0.059 |

Note: \*: C: Coarse grained; F: Fine grained.

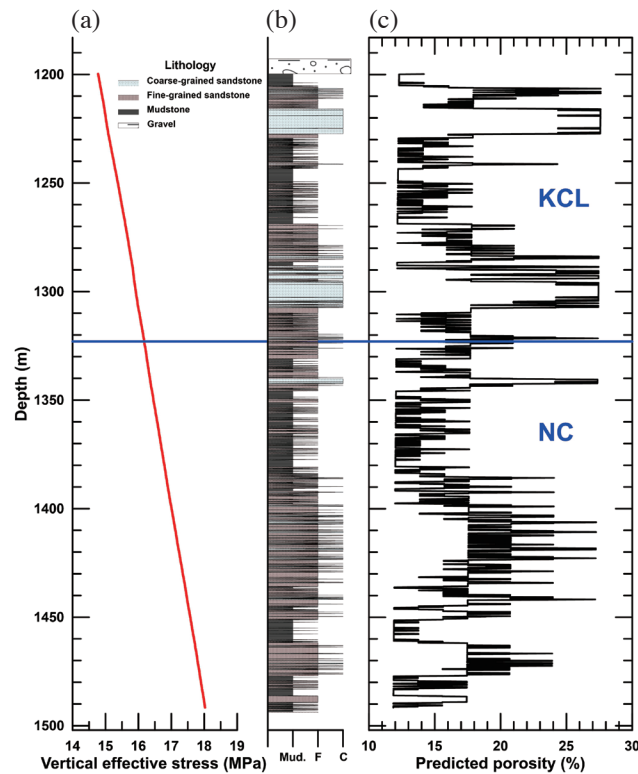


Fig. 5. Vertical effective stress (a), lithology (b), and predicted porosity (c) of the potential CO<sub>2</sub> geosequestration site near well KY-1. The depths of 1199.72 - 1492.72 m are projected from well Sanying-1 (SY-1; depths of 7 - 300 m, Fig. 3). Note that the vertical effective stress is derived from Eq. (4). KCL represents the Kueichulin Formation; NC represents the Nanchuang Formation. (Color online only)

rock types encountered in borehole Sanying-1 are coarse-grained and fine-grained sandstones and mudstones, based on the gamma-ray logs (< 65, 65 - 110, and 110 - 200 counts per second, respectively). These rock type classifications (Fig. 5b) reasonably match those based on the visual observations (Fig. 3b). Average parameters to be used in the stress-history-dependent porosity model were calculated for each lithology. The average parameters ( $\phi_o$  and  $q$ ) required to evaluate the porosity-depth relationship in normally consolidated rocks are shown in Table 4.

The porosity at various depths was calculated using Eq. (1) with the parameters listed in Table 4. The porosity-depth relationship of the normally consolidated rocks with the three lithologies (Fig. 5b) is shown in Fig. 5c. The predicted porosity-depth relationship is for rocks at depths between 1199.72 and 1492.72 m in well KY-1. The predicted porosities (at 0.1-m intervals) are plotted using a running average with an increment of 0.3 m. The calculated porosities of the coarse-grained sandstones range from 27.61 - 27.20%, the calculated porosities of the fine-grained sandstones range from 17.97 - 17.43%, and the calculated porosities of the mudstones are in the 12.29 - 11.85% range. Most of the variation in porosity appears to be controlled by the combination of rock types (seven different porosities out of ten combinations are apparent in the running averages). The porosities decreased slightly with increasing burial depths, which is associated with increasing vertical effective stresses. Accordingly, the porosity-depth relationships of the rocks to a depth of approximately one kilometer can be predicted using samples from a shallow borehole from potential CO<sub>2</sub> reservoirs that have been uplifted to near the ground surface.

## 5. DISCUSSION

### 5.1 Influence of Stress History on Porosity-Depth Relationship in Normally and Overconsolidated Rocks

In this section, we demonstrate the stress history influence on rock porosity estimates during maximum burial depth using laboratory-measured rock porosities from rocks recovered from uplifted formations (herein, we refer to these rocks as over-consolidated). We illustrate this influence based on the assumption of a rock succession consisting of uniform coarse-grained sandstones. The eroded thickness of the overlying strata is assumed to be 2500 m, as inferred from the depth-contour map of the top of the Nanchuang Formation shown in Lin and Watts (2002). Accordingly, the effective stress the in-situ rocks experienced during their maximum burial was 35.46 MPa. The parameters ( $\phi_o$ ,  $q$ , and  $q'$ ) of sample SY1-01 listed in Table 3 were selected to calculate the porosity-depth relationship. Other parameters for the synthetic case are shown in Table 5.

Equation (3) can be used to evaluate the porosity of

the over-consolidated rocks at various depths and hence the various effective stresses after their unloading to atmospheric pressure. This situation is present when evaluating the porosity-depth relationship in rock cores measured under atmospheric pressure using a core logger, in which case the in-situ effective stress is neglected. Second, the influence of the in-situ effective stress on the porosity is considered. This situation is present when the density or sonic log is used to derive the porosity-depth relationship in the rocks. Because the overlying formation was uplifted and eroded in our hypothetical case, the uplift and erosion effects were not considered under this condition. To predict the porosity-depth relationship in normally consolidated rocks, the stress history influence should be considered using a shallow borehole drilled through an over-consolidated formation. In this instance, Eq. (1) may be used to calculate the porosity-depth relationship of normally consolidated rocks (proposed method in this study).

Three different approaches for deriving the porosity-depth relationship are summarized as follows: (i) using the porosity measured with the core logger under atmospheric pressure; (ii) using the porosity measured by the density or sonic logging, in which case the uplift and erosion effects are neglected; and (iii) the porosity derived using the proposed model.

Figure 6a shows the porosity variation in a coarse-grained sandstone, the synthetic case, at depths of 800 - 1200 m using the three different methods. If the porosity measured under atmospheric pressure is used to estimate the porosity of coarse-grained sandstones at depth, the porosity (29.51 - 29.30%) will be significantly overestimated (solid line in Fig. 6a) compared to the porosity measured using borehole logging, which neglects the uplift and erosion effects (long dashed line) and porosity derived using the proposed method (short dashed line). Therefore, a core logger should be used with caution when determining the porosity

Table 4. Average parameters of various lithologies in the stress-history-dependent porosity model.

|          | Coarse-grained sandstone | Fine-grained sandstone | Mudstone |
|----------|--------------------------|------------------------|----------|
| $\phi_o$ | 43.74%                   | 38.33%                 | 30.60%   |
| $q$      | 0.092                    | 0.152                  | 0.183    |

Table 5. Parameters of the synthetic uniform formation.

| Parameters                    | Value                    |
|-------------------------------|--------------------------|
| Bulk density                  | 2.446 g cm <sup>-3</sup> |
| Present depth                 | 800 - 1200 m             |
| Maximum burial depth          | 3300 - 3700 m            |
| Eroded thickness (overburden) | 2500 m (35.46 MPa)       |

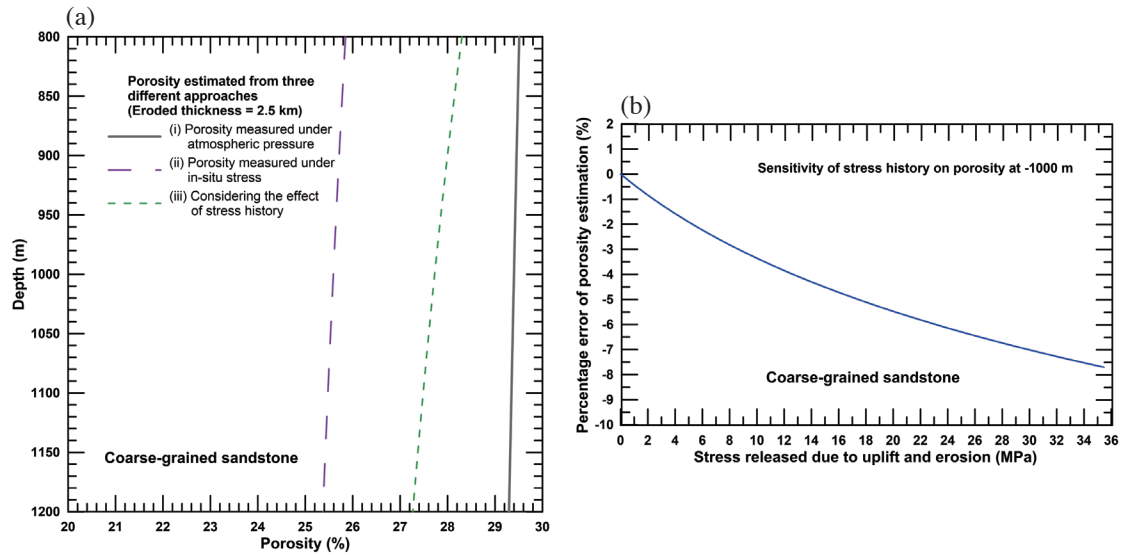


Fig. 6. (a) The porosity-depth curves of the synthetic case derived from different approaches. (i) Porosity measured under atmospheric pressure: predicted relationship from an over-consolidated rock using core loggers (porosity measurement under atmospheric pressure); (ii) porosity measured neglecting the effect of uplift and erosion: predicted relationship from an over-consolidated rock using borehole loggers (porosity measurement under in-situ stress); (iii) porosity derived using the proposed method: predicted relationship of a normally consolidated rock from porosity measurement of over-consolidated rocks (considering the stress history effect). (b) The percentage error in porosity estimates induced by neglecting the stress history effect (various stresses reduced due to uplift and erosion) of the synthetic case at a depth of 1000 m. (Color online only)

and estimating the storage capacity of a target formation.

A comparison of the porosity-depth relationship determined using borehole logging, which neglects the uplift and erosion effects and the porosity-depth relationship determined using the proposed method indicates that the influence of the stress history is also significant. If the porosity determined using the borehole logger in over-consolidated rocks is used to predict the porosity-depth relationship in normally consolidated rocks, the results will be underestimated. The influence of the stress history on the porosity-depth relationship is further illustrated in Fig. 6b. The vertical axis is the percentage error of the estimation if the stress history influence (stresses released due to uplift and erosion) is neglected. This percentage error of the estimation is defined by “(porosity estimated by approach ii minus porosity estimated by approach iii) divided by porosity estimated by approach iii”. When the stress released due to uplift and erosion is 0 MPa, the percentage error is 0. With increasing released stress, the percentage error of the estimated porosity is increased if the stress history is neglected. If the stress released due to uplift and erosion is 35.46 MPa (burial depth is approximately 3.5 km), the estimating percentage error due to neglecting the stress history is 7.7%.

## 5.2 The Injection Pressure Impact on Estimated Rock Porosities

CO<sub>2</sub> injection into rock formations displaces and/or compresses existing formation fluid. The injection pressure will be greater than the hydrostatic pressure, at least at depths

where the CO<sub>2</sub> is injected (Holloway and van der Straaten 1995). The CO<sub>2</sub> injection pressure effect on the porosity at various depths was further investigated. Note that injection pressure in excess of the hydrostatic pressure is referred to as the “injection pressure” in the following discussion.

Figure 7a shows the porosity-depth curves for the synthetic uniform coarse-grained sandstone corresponding to injection pressures of 0 (or neglecting the influence of injection pressure), 2, 3, 4, 5, and 6 MPa higher than the hydrostatic pressure. The proposed method was used to determine the porosity-depth relationship based on an assumed stress released due to uplift and erosion of 35.46 MPa. There is a clear trend of increasing porosities with increasing injection pressures. This trend indicates that the porosity of the target formations during CO<sub>2</sub> injection will increase due to the injection pressure. Meanwhile, the difference between the porosities before and after injection decreases with increasing depth.

Figure 7b shows the percentage error in the predicted rock porosity at a depth of 1000 m if the injection pressure effect is neglected. A significant percentage error (6.7%) in the estimated porosity is induced by a large injection pressure (13 MPa), where the percentage error is defined as “(estimated porosity considering injection pressure minus estimated porosity neglecting injection pressure) divided by estimated porosity considering injection pressure”. These results indicate that the injection pressure effect on the porosity becomes measurable as the injection pressure increases. Although it is well understood that other important factors, such as the CO<sub>2</sub> density and irreducible water saturation,

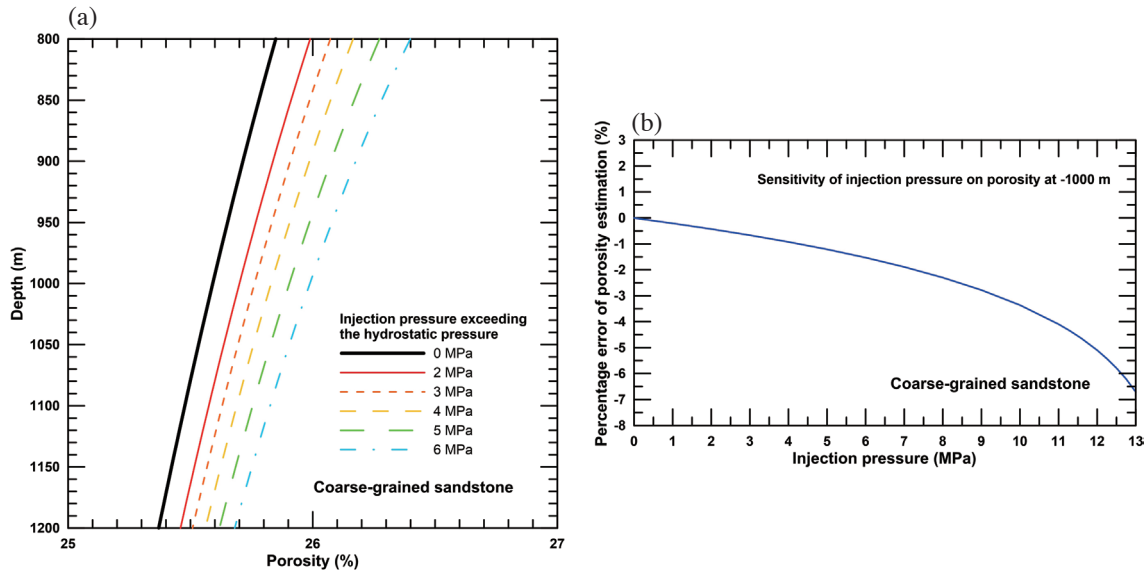


Fig. 7. (a) The porosity-depth curve of the synthetic case before injection (or neglecting the influence of injection pressure) and porosity-depth curves under various injection pressure (2, 3, 4, 5, and 6 MPa larger than the hydrostatic pressure). (b) The percentage porosity estimate error for an over-consolidated rock at 1000 m depth if the  $\text{CO}_2$  injection pressure effect (injection pressure in excess of the hydrostatic pressure) is neglected. (Color online only)

dominate the storage capacity, the injection pressure influence, and the stress history experienced by the rocks on the target formation porosity should still be considered when estimating the  $\text{CO}_2$  storage volume.

## 6. CONCLUSIONS

We used a stress-history-dependent porosity model to evaluate the stress history influence on  $\text{CO}_2$  storage capacity estimates in a potential sedimentary basin aquifer in north-western Taiwan. The proposed method was used to predict the porosity-depth relationship of a deep target formation using available data from a shallow borehole. The primary conclusions are summarized as follows:

- (1) The porosity of samples based on laboratory tests under atmospheric pressure was significantly larger than the porosity under the in-situ stress. It is strongly recommended that the  $\text{CO}_2$  storage capacity not be estimated from the porosity measured under atmospheric pressure.
- (2) The porosity-depth relationship of rocks can be obtained from borehole densities or velocity logger data. However, the uplift and erosion effects on the measured porosity must to be carefully evaluated.
- (3) Neglecting the stress history effect on the porosity of over-consolidated rocks may induce errors ( $\sim 7.7\%$  for the synthetic case when the stress released due to uplift and erosion is 35.46 MPa; i.e., the eroded thickness is approximately 3.5 km) when predicting the porosity-depth relationship of normally consolidated rocks. Based on the laboratory measurements and a stress-history-dependent porosity model, the porosity measurement of over-

consolidated rocks (in the hanging wall of a thrust fault) could be used to estimate the porosity-depth relationship of the normally consolidated sedimentary rocks. Accordingly, the rock samples from a shallow boring in the exposed target formation may be used to estimate the  $\text{CO}_2$  storage capacity in a deep saline aquifer while considering the stress history effect on the porosity of sedimentary rocks.

- (4) The pore pressure buildup during  $\text{CO}_2$  injection will induce an increase in the rock porosity. A significant percentage error (6.7%) in the estimated porosity will be induced by a large injection pressure (13 MPa) in rock at a depth of 1000 m if the injection pressure effect is neglected. These results indicate that the injection pressure effect on the porosity becomes measurable as the injection pressure increases. Although this amount is not significant, this research indicates that the storage capacity estimate will be slightly conservative if the injection pressure influence on the rock porosity is neglected.

**Acknowledgements** The authors would like to thank the Ministry of Science and Technology of the Republic of China, Taiwan for financially supporting this research under contracts No. NSC 102-3113-P-008-009 and MOST-105-3113-E-008-009. We would also like to extend our sincere thanks to anonymous reviewers for their very constructive comments, which greatly improved the manuscript.

## REFERENCES

Athy, L. F., 1930: Density, porosity, and compaction of

- sedimentary rocks. *AAPG Bull.*, **14**, 1-24.
- Bachu, S., 2000: Sequestration of CO<sub>2</sub> in geological media: Criteria and approach for site selection in response to climate change. *Energ. Convers. Manage.*, **41**, 953-970, doi: 10.1016/S0196-8904(99)00149-1. [[Link](#)]
- Bachu, S., 2008: CO<sub>2</sub> storage in geological media: Role, means, status and barriers to deployment. *Progr. Energ. Combust. Sci.*, **34**, 254-273, doi: 10.1016/j.pecs.2007.10.001. [[Link](#)]
- Bachu, S., D. Bonijoly, J. Bradshaw, R. Burruss, S. Holloway, N. P. Christensen, and O. M. Mathiassen, 2007: CO<sub>2</sub> storage capacity estimation: Methodology and gaps. *Int. J. Greenh. Gas Con.*, **1**, 430-443, doi: 10.1016/S1750-5836(07)00086-2. [[Link](#)]
- Benson, S. M. and D. R. Cole, 2008: CO<sub>2</sub> sequestration in deep sedimentary formations. *Elements*, **4**, 325-331, doi: 10.2113/gselements.4.5.325. [[Link](#)]
- Birkholzer, J. T. and Q. Zhou, 2009: Basin-scale hydrogeologic impacts of CO<sub>2</sub> storage: Capacity and regulatory implications. *Int. J. Greenh. Gas Con.*, **3**, 745-756, doi: 10.1016/j.ijggc.2009.07.002. [[Link](#)]
- Bradshaw, J., S. Bachu, D. Bonijoly, R. Burruss, S. Holloway, N. P. Christensen, and O. M. Mathiassen, 2007: CO<sub>2</sub> storage capacity estimation: issues and development of standards. *Int. J. Greenh. Gas Con.*, **1**, 62-68, doi: 10.1016/S1750-5836(07)00027-8. [[Link](#)]
- Chiu, W. Y., 2009: Oligocene to Pleistocene basin development and sequence stratigraphy in northwest Taiwan. Master Thesis, National Central University, Taoyuan City, Taiwan, 114 pp. (in Chinese)
- Dong, J. J., J. Y. Hsu, W. J. Wu, T. Shimamoto, J. H. Hung, E. C. Yeh, Y. H. Wu, and H. Sone, 2010: Stress-dependence of the permeability and porosity of sandstone and shale from TCDP Hole-A. *Int. J. Rock Mech. Min. Sci.*, **47**, 1141-1157, doi: 10.1016/j.ijrmms.2010.06.019. [[Link](#)]
- Holloway, S. and R. van der Straaten, 1995: The Joule II project: The underground disposal of carbon dioxide. *Energ. Convers. Manage.*, **36**, 519-522, doi: 10.1016/0196-8904(95)00057-K. [[Link](#)]
- IPCC, 2005: IPCC Special Report on Carbon Dioxide Capture and Storage, Prepared by Working Group III of the Intergovernmental Panel on Climate Change, Cambridge University Press, Cambridge, United Kingdom and New York, NY, USA, 442 pp.
- Juanes, R., E. J. Spiteri, F. M. Orr Jr., and M. J. Blunt, 2006: Impact of relative permeability hysteresis on geological CO<sub>2</sub> storage. *Water Resour. Res.*, **42**, W12418, doi: 10.1029/2005WR004806. [[Link](#)]
- Kharaka, Y. K., D. R. Cole, S. D. Hovorka, W. D. Gunter, K. G. Knauss, and B. M. Freifeld, 2006: Gas-water-rock interactions in Frio Formation following CO<sub>2</sub> injection: Implications for the storage of greenhouse gases in sedimentary basins. *Geology*, **34**, 577-580, doi: 10.1130/G22357.1. [[Link](#)]
- Lackner, K. S., 2003: A guide to CO<sub>2</sub> sequestration. *Science*, **300**, 1677-1678, doi: 10.1126/science.1079033. [[Link](#)]
- Lengler, U., M. De Lucia, and M. Kühn, 2010: The impact of heterogeneity on the distribution of CO<sub>2</sub>: Numerical simulation of CO<sub>2</sub> storage at Ketzin. *Int. J. Greenh. Gas Con.*, **4**, 1016-1025, doi: 10.1016/j.ijggc.2010.07.004. [[Link](#)]
- Lin, A. T. and A. B. Watts, 2002: Origin of the West Taiwan basin by orogenic loading and flexure of a rifted continental margin. *J. Geophys. Res.*, **107**, doi: 10.1029/2001JB000669. [[Link](#)]
- Lin, A. T., A. B. Watts, and S. P. Hesselbo, 2003: Cenozoic stratigraphy and subsidence history of the South China Sea margin in the Taiwan region. *Basin Res.*, **15**, 453-478, doi: 10.1046/j.1365-2117.2003.00215.x. [[Link](#)]
- Morris, J. P., Y. Hao, W. Foxall, and W. McNab, 2011: A study of injection-induced mechanical deformation at the In Salah CO<sub>2</sub> storage project. *Int. J. Greenh. Gas Con.*, **5**, 270-280, doi: 10.1016/j.ijggc.2010.10.004. [[Link](#)]
- Oldenburg, C. M., K. Pruess, and S. M. Benson, 2001: Process modeling of CO<sub>2</sub> injection into natural gas reservoirs for carbon sequestration and enhanced gas recovery. *Energ. Fuel.*, **15**, 293-298, doi: 10.1021/ef000247h. [[Link](#)]
- Rohmer, J. and D. M. Seyed, 2010: Coupled large scale hydromechanical modelling for caprock failure risk assessment of CO<sub>2</sub> storage in deep saline aquifers. *Oil Gas Sci. Technol. - Rev. IFP*, **65**, 503-517, doi: 10.2516/ogst/2009049. [[Link](#)]
- Rutqvist, J. and C. F. Tsang, 2002: A study of caprock hydromechanical changes associated with CO<sub>2</sub>-injection into a brine formation. *Environ. Geol.*, **42**, 296-305, doi: 10.1007/s00254-001-0499-2. [[Link](#)]
- Rutqvist, J., J. Birkholzer, F. Cappa, and C. F. Tsang, 2007: Estimating maximum sustainable injection pressure during geological sequestration of CO<sub>2</sub> using coupled fluid flow and geomechanical fault-slip analysis. *Energ. Convers. Manage.*, **48**, 1798-1807, doi: 10.1016/j.enconman.2007.01.021. [[Link](#)]
- Rutqvist, J., J. T. Birkholzer, and C. F. Tsang, 2008: Coupled reservoir-geomechanical analysis of the potential for tensile and shear failure associated with CO<sub>2</sub> injection in multilayered reservoir-caprock systems. *Int. J. Rock Mech. Min. Sci.*, **45**, 132-143, doi: 10.1016/j.ijrmms.2007.04.006. [[Link](#)]
- Rutqvist, J., D. W. Vasco, and L. Myer, 2010: Coupled reservoir-geomechanical analysis of CO<sub>2</sub> injection and ground deformations at In Salah, Algeria. *Int. J. Greenh. Gas Con.*, **4**, 225-230, doi: 10.1016/j.ijggc.2009.10.017. [[Link](#)]
- Terzaghi, K., 1943: Theoretical Soil Mechanics, John Wiley & Sons, Inc., Hoboken, NJ, USA, 528 pp, doi:

- 10.1002/9780470172766. [Link]
- Torp, T. A. and J. Gale, 2004: Demonstrating storage of CO<sub>2</sub> in geological reservoirs: The Sleipner and SACS projects. *Energy*, **29**, 1361-1369, doi: 10.1016/j.energy.2004.03.104. [Link]
- Vilarrasa, V., D. Bolster, S. Olivella, and J. Carrera, 2010: Coupled hydromechanical modeling of CO<sub>2</sub> sequestration in deep saline aquifers. *Int. J. Greenh. Gas Con.*, **4**, 910-919, doi: 10.1016/j.ijggc.2010.06.006. [Link]
- Wang, J. H., J. H. Hung, and J. J. Dong, 2009: Seismic velocities, density, porosity, and permeability measured at a deep hole penetrating the Chelungpu fault in central Taiwan. *J. Asian Earth Sci.*, **36**, 135-145, doi: 10.1016/j.jseaes.2009.01.010. [Link]
- Wilson, E. J., T. L. Johnson, and D. W. Keith, 2003: Regulating the ultimate sink: Managing the risks of geologic CO<sub>2</sub> storage. *Environ. Sci. Technol.*, **37**, 3476-3483, doi: 10.1021/es021038+. [Link]
- Wu, W. J. and J. J. Dong, 2012: Determining the maximum overburden along thrust faults using a porosity versus effective confining pressure curve. *Tectonophysics*, **578**, 63-75, doi: 10.1016/j.tecto.2011.12.028. [Link]
- Xu, T., E. Sonnenthal, N. Spycher, and K. Pruess, 2006: TOUGHREACT-A simulation program for non-isothermal multiphase reactive geochemical transport in variably saturated geologic media: Applications to geothermal injectivity and CO<sub>2</sub> geological sequestration. *Comput. Geosci.*, **32**, 145-165, doi: 10.1016/j.cageo.2005.06.014. [Link]
- Yang, K. M., S. T. Huang, H. H. Ting, J. C. Wu, W. R. Chi, W. W. Mei, H. H. Hsu, and T. H. Hsuan, 2003: Study of fault structures in foothills belt and deformation front, Taiwan. *Exploration and Production Research Bulletin*, **25**, 45-72. (in Chinese)